Research Article

Catalytic degradation of methylene blue by iron nanoparticles synthesized using *Galinsoga parviflora*, *Conyza bonariensis* and *Bidens pilosa* leaf extracts

Sammy Indire Wanakai[1] · **Patrick Gachoki Kareru**[1] · **David Sujee Makhanu**[2] · **Edwin Shigwenya Madivoli**[1] · **Ernest Gachui Maina**[1] · **Augustine Otieno Nyabola**[1]

Abstract

Green synthesized metallic nanoparticles are environmentally friendly, bio-compatible, and highly stable. The aim of this study was to synthesize iron nanoparticles (FeNPs) from $FeCl_3$ solution using aqueous leaf extracts of *Galinsoga parviflora* (Gp), *Conyza bonariensis* (Cb) and *Bidens pilosa* (Bp) and use them in degradation of methylene blue dye. The iron nanoparticles were characterized using UV–Vis spectrophotometer, FT-IR spectrophotometer, X-ray Fluorescence (EDXRF), X-ray diffractometer (XRD), and scanning electron microscope (SEM). Phytochemical screening for presence of secondary metabolites revealed presence of phenolics, phytosterols and flavonoids. The total phenolic and flavonoid content in *Galinsoga parviflora*, *Conyza bonariensis* and *Bidens pilosa* leaf extracts were 57.67 ± 1.27, 117.13 ± 0.03, 126.27 ± 0.013 mg Gallic Equivalent/g of Dry Weight (mg GAE/g DW) and 39.00 ± 0.56, 45.50 ± 0.59, 33.13 ± 0.81 mg Rutin Equivalent/g of Dry Weight (mg RE/g DW) respectively. The UV–Vis spectrum of $FeCl_3$ had a shoulder at 320 nm, which disappeared upon addition of *G. parviflora*, *C. bonariensis* and *B. pilosa* extracts confirming formation of iron nanoparticles. Evaluation of iron content of the synthesized nanoparticles revealed that the iron content in *G. parviflora*, *C. bonariensis* and *B. pilosa* extracts was 51, 47 and 44% respectively. XRD data revealed presence of a large amorphous coating that masked iron peaks, though 2 theta values observed have been reported to be of iron oxides. Methylene blue degradation studies revealed that CbNPs, BpNPs and GpNPs synthesized were good biocatalysts as they degraded the dye by 86, 84.3 and 92% respectively. Therefore, green synthesized iron nanoparticles is cost effective and environmentally safe in providing insight in the environmental removal of dyes.

Keywords *Bidens pilosa* · Secondary metabolites · Iron nanoparticles · Biosynthesis · Degradation

1 Introduction

Green synthesized metallic nanoparticles exhibit unique physical, thermal, chemical, and catalytic properties, [1, 2] and have found great application in health care as antiplasmodial [3], anticancer, and antimicrobial [4, 5], synthetic biology and cellular transportation [6]. The most important feature responsible for their wide range use is attributed to their large surface area to volume ratio, stability, biocompatibility and have a high surface energy as well as unique adsorption phenomenon [7-9]. In addition, metal nanoparticles are a few hundred nanometers smaller than comparable large biological molecules such as enzymes, receptors and antibodies [1]. The unique physical and chemical properties of metal nanoparticles may lead to effective interactions between itself, bacterial cell membrane and other biological entities [1, 10]. The antimicrobial activity of nanoparticles is

✉ Sammy Indire Wanakai, wanakaisammy@gmail.com | [1]Chemistry Department, Jomo Kenyatta University of Agriculture and Technology, P.O. Box 62,000-00200, Nairobi, Kenya. [2]Department of Biological & Physical Sciences, Karatina University, P.O. Box 1957-10101, Karatina, Kenya.

not well understood, however, various mechanisms have been suggested. The nanoparticles have been reported to cause oxidative stress to the cell of the gram-negative bacteria by generating excess reactive oxygen species [11] as well as release of antimicrobial metal ions from the surface of the nanoparticle. The nanoparticles also have a membrane damaging abrasiveness which inherently gives them an antimicrobial property [12].

Plants exhibit high chemical diversity due to genetic variations, ecological and environmental factors [6]. This means that the plant extracts will contain different concentrations of natural reducing agents which can influence the characteristics of the nanoparticles. Green synthesized iron oxide nanoparticles from plants offers an alternative for exploitation of plants for pharmaceutical, water treatment, biomedical and catalytic applications [13-17]. Previous studies have shown that iron nanoparticles produced from plants have been used to catalyze the degradation of organic dyes such as bromothymol blue, methylene blue, aniline and Rhodamine B [14, 18]. The iron nanoparticles have shown much efficiency in the oxidation of organic dyes. This is because iron has two stable oxidation states which influence the efficiency of iron nanoparticles as photo catalysts [16, 19]. Its suggested that the mechanism for photocatalytic degradation involves oxidation of the dye by hydrogen peroxide, catalyzed by iron oxides and hydroxides present in the nanoparticles through a Fenton like mechanism. This involves corrosion of the surface of the iron oxide nanoparticle in an acidic environment producing ferrous ions that generate hydroxyl radicals. The radicals attack the dye molecules thus degrading them [14, 20].

In this study, plant mediated iron nanoparticles (FeNPs) were synthesized using extracts of local herbal plants *Galinsoga parviflora*, *Conyza bonariensis* and *Bidens pilosa* leaf extracts as reducing and stabilizing agents. These plants were chosen basing on their availability as well as the presence of large amounts of biodegradable and water soluble polyphenols which aid in the synthesis of the nanoparticles through reduction as well as stabilization [8, 21, 22]. The synthesis of iron nanoparticles was performed in a one-step by adding the plant extracts to 0.1 M of ferric chloride as the iron precursor leading to formation of a black precipitate of *Galinsoga parviflora* (GpNPs), *Conyza bonariensis* (CbNPs) and *Bidens pilosa* (BpNPs) iron particles. These were analysed using UV–Vis spectrophotometer (UV–VIS), Fourier Transform Infrared spectrophotometer, X-ray Fluorescence (EDXRF), X-ray diffractometer (XRD), and scanning electron microscope (SEM) to determine composition, structure and size. The iron nanoparticles were then used as catalysts in the degradation of methylene blue solution.

2 Materials and methods

2.1 Collection of plant extracts

Fresh leafs of *Galinsoga Parviflora, Bidens pilosa* and *Conyza bonariensis* were collected from Bungoma East Sub-County, Bungoma County in Kenya, washed thoroughly with running laboratory tap water and further with distilled water and air-dried at room temperature (20–25 °C) for 14 days to remove moisture [23]. Dry plant materials were ground finely using a milling machine.

2.2 Quantitative Phytochemical analysis

2.2.1 Total phenolic content

The total phenolic content of the crude extracts was evaluated by the Folin–Ciocalteau method with some modifications using Garlic acid as standard [24]. Dry and ground plant material (0.1 g) were extracted using 4.9 mL 80% methanol and filtered through a Whatman filter paper no.1 to make the stock sample. Absorbance was measured at 769 nm using compact, double-beam UV–Vis spectrophotometer (UV 1800, Shimadzu) [25, 26]. The total phenolic content expressed in mg of garlic acid equivalents (GAE)/g of dry weight extract (DW).

2.2.2 Total flavonoid content

The total flavonoid content was determined using the Aluminium chloride method with Rutin as the standard according to [27] and the absorption readings done at 510 nm using compact, double-beam UV–Vis spectrophotometer (UV 1800, Shimadzu). The calibration curve was used to determine the total flavonoid content and was expressed as mg of Rutin equivalent (RE)/g of dry weight of sample.

2.2.3 Synthesis of iron nanoparticles from leaf extract

Twenty grams of the dried and ground *Galinsoga parviflora*, *Conyza bonariensis* and *Bidens pilosa* were transferred into different labeled 250 mL volumetric flasks. 200 mL of distilled water added and the mixture boiled at 70 °C with constant stirring for 45 min. The cooled extract was collected by filtering three times with cotton wool and further through Whatman No.1 filter paper to get a clear extract [7, 13, 28]. 0.1 M $FeCl_3 \cdot 6H_2O$ solution (working standard) was prepared by weighing 13.52 g of $FeCl_3 \cdot 6H_2O$ and dissolving in 100 mL of distilled water and further topped to 500 mL with enough distilled water [29]. Synthesis of Iron nanoparticles was done

by adding 30 mL of plant extracts to 10 mL of 0.1 M Ferric Chloride dropwise using a burette [30, 31] with constant stirring at room temperature and pressure. The black precipitate was washed several times with distilled water, centrifuged at 6000 rpm for 10 min (Centurion 6000). The obtained nanoparticles were dried at 60 °C in the oven [29].

2.2.4 Characterization of iron nanoparticles

UV–Vis absorption spectra were recorded using compact, double-beam UV–Vis spectrophotometer (UV 1800, Shimadzu) in the range of 200–800 nm [32]. The Shimadzu FTIR spectrophotometer (FTS—8000, Japan) was used to analyze functional groups present on the plant extract as well as the iron nanoparticles by the standard KBr method, with spectral resolution set at 4 cm^{-1} and the scanning range from 400 to 4000 cm^{-1} [33]. The elemental composition was done using the X-ray fluorescence machine Bruker model at the Mines and Geological Department laboratories, Kenya. The crystallinity phase identified using STOE STADIP P X-ray Powder Diffraction System (STOE & Cie GmbH, Darmstadt, Germany). The X-ray generator was equipped with a copper tube operating at 40 kV and 40 mA and the sample irradiated with a monochromatic Cu Kα radiation with a wavelength of 1.5409 nm and 2θ range of 2–90 °C at 0.05 °C intervals. Morphological analysis was performed using Tescan Mira3 LM FE Scanning electron microscope, Germany operated at an accelerating voltage of 3 kV. The samples were gold sputtered before observation to avoid the charging effect.

2.2.5 Methylene blue degradation

Methylene blue degradation was established using previous methodology [34]. The reagent was prepared by diluting 1 mL of it to 50 mL with distilled water. Two spectral scans were done on 3 mL of the solution in the range of 800–300 nm in 5 min intervals using double-beam UV–Vis spectrophotometer (UV 1800, Shimadzu). 1 mL Hydrogen peroxide was added and two more scans were allowed, after which 50 mg of the iron nanoparticles were sprinkled on the solution and allowed to run for 10.5 h in 5 min intervals. A spectral scan for the degradation of methylene blue solution using hydrogen peroxide without the nanoparticles and nanoparticles alone as a control was done under the same conditions for 1 h.

3 Results and discussion

3.1 Biosynthesis of iron nanoparticles

Figure 1 shows the schematic representation of biosynthesis of iron nanoparticles. The colour changes indicated the formation of iron nanoparticles [7].

The results indicated a relatively higher concentration of the total flavonoids as compared to total phenolic content. *Conyza bonariensis* had the highest total phenols (45.50 ± 0.59) while *Bidens pilosa* had the highest total flavonoids (126.27 ± 0.01). Polyphenols in plants are responsible for the antioxidant behaviour of most plants and offer the potential of using plants as nutraceuticals as well as food additives. As discussed in the mechanism of nanoparticles formation [35, 36], the phytochemicals present offer a complementary role in the reduction as well as stabilization of the iron nanoparticle [37]. The postulate underlying the green synthesis perspective is that the phytochemicals present in the plant naturally reduce as well as stabilize the nanoparticle [36–39] (Table 1).

3.2 UV–Vis absorption spectra

UV–Vis absorption spectra of an aqueous solution of *Galinsoga Parviflora*, *Bidens pilosa* and *Conyza bonariensis* leaf extracts, synthesized iron nanoparticles and iron III chloride Figs. 2, 3, 4.

The leaf extracts were brown in colour and had higher absorption peaks at 267 nm, 288 nm and 286 nm for *Galinsoga parviflora*, *Bidens pilosa* and *Conyza bonariensis* respectively. These indicates that the leaf extracts contain electron rich polyphenols, amino acids as well as sugars which are responsible for the reduction of Fe^{3+} [18, 40]. Fe^{3+} spectra displayed peaks at absorption peaks of 203 nm and 295 nm. Upon the addition of the extract into the 0.1 M Ferric chloride solution, black colored colloidal solutions developed gradually. The strong absorption peaks of the extract, and the Fe^{3+} in
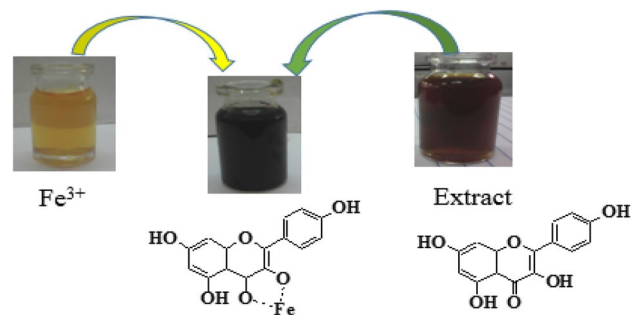

Fig. 1 Flow diagram for synthesis of iron nanoparticles

Table 1 Quantitative total phenolic and total flavonoid content of *Galinsoga Parviflora, Bidens pilosa* and *Conyza bonariensis* leaf extracts

Sample/extracts	Total phenols (mg gallic acid equivalent/g dry weight)	Total flavonoids (mg rutin equivalent/g dry weight)
Galinsoga parviflora	39.00 ± 0.56	57.67 ± 1.27
Bidens pilosa	33.13 ± 0.81	126.27 ± 0.01
Conyza bonariensis	45.50 ± 0.59	117.13 ± 0.03
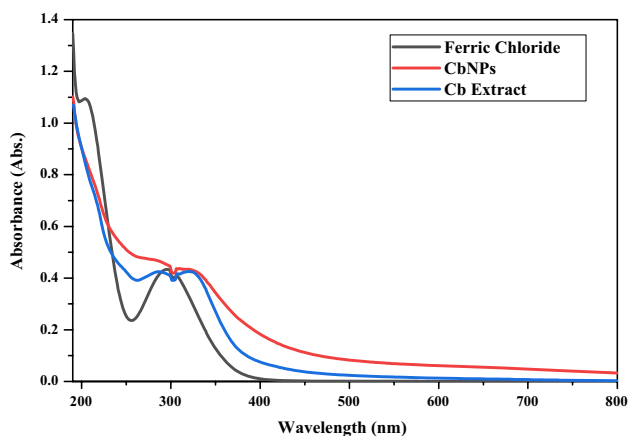
Fig. 2 UV–Visible absorption spectrum of iron III chloride (Fe^{3+}), *Conyza bonariensis* (Cb) leaf extracts and synthesized iron nanoparticles
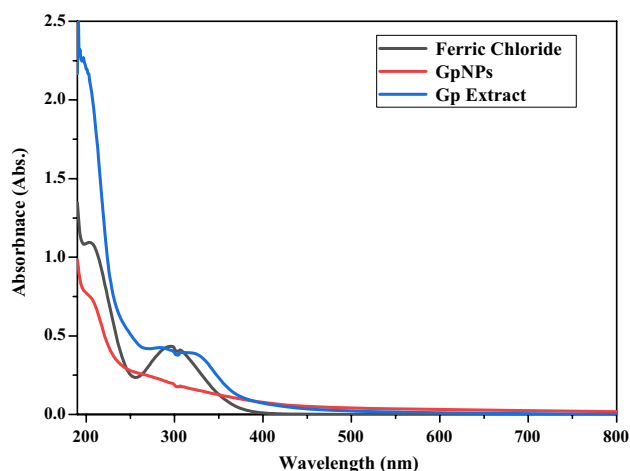
Fig. 4 UV–Visible absorption spectrum of iron III chloride (Fe^{3+}), *Galinsoga Parviflora* (Gp) leaf extracts and synthesized iron nanoparticles
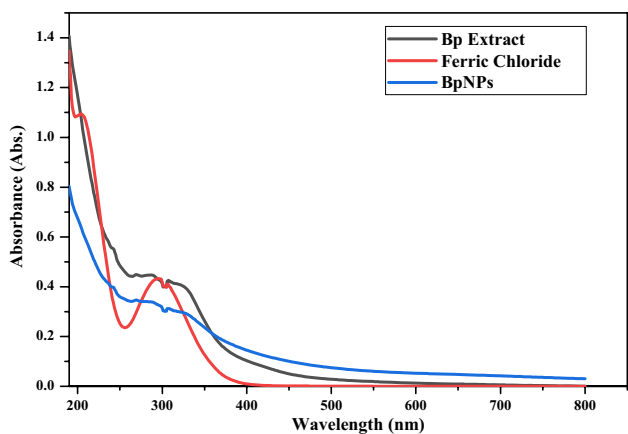

Fig. 3 UV–Visible absorption spectrum of iron III chloride (Fe^{3+}), *Bidens pilosa* (Bp) leaf extracts and synthesized iron nanoparticles
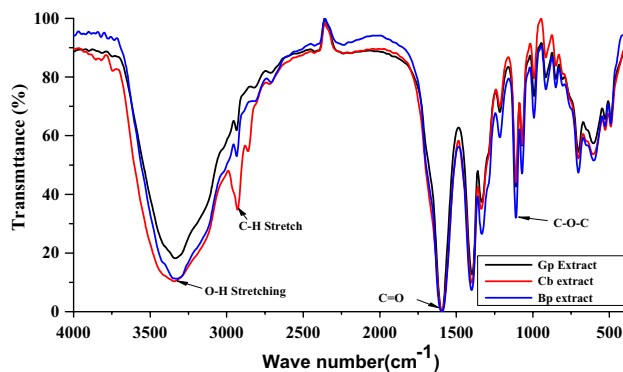

Fig. 5 FTIR spectra of *Conyza bonariensis* (Cb extract), *Galinsoga parviflora* (Gp extract) and *Bidens pilosa* (Bp extract)

3.3 FTIR characterization of ZVIN

The functional groups present in the nanoparticles as well as the aqueous leaf extracts were determined using FTIR and Figs. 5 and 6 shows the spectra obtained respectively.

Based on the spectra obtained (Fig. 5), the *Conyza bonariensis, Galinsoga parviflora* and *Bidens pilosa* extracts depicted O–H stretching of phenolic groups at 3309 cm^{-1} 3329.7 cm^{-1} and 3336 cm^{-1} respectively. This is suggested

the range of 200 to 350 nm disappeared, and a broad absorption was observed, which demonstrate the formation of poly dispersed iron nanoparticles through electron transfer and surface Plasmon resonance [41]. The change in color is associated with the excitation of electrons as the Fe^{3+} ions are reduced to Fe^0 [18].
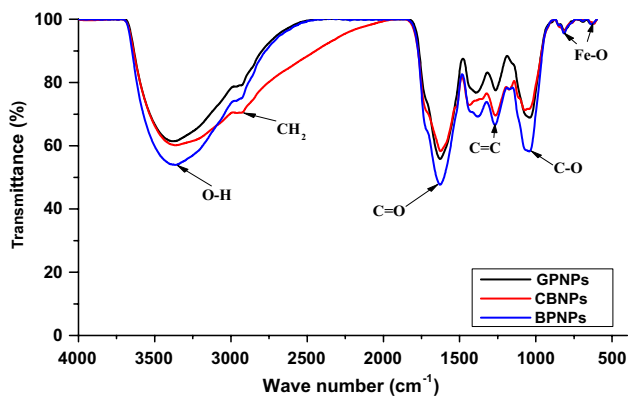
Fig. 6 FTIR spectra of *Conyza bonariensis* iron nanoparticles (CbNPs), *Galinsoga parviflora* iron nanoparticles (GpNPs) and *Bidens pilosa* iron nanoparticles (BpNPs)

Fig. 7 FTIR spectra of BpNPs, CbNPs and GpNPs after degradation of methylene blue solution using hydrogen peroxide

to be responsible for the bioreducton of the ferric ions [42]. The O–H stretching vibration in CbNPs, GpNPs and BpNPs shifted to 3406 cm^{-1}, 3438.3 cm^{-1} and 3402.6 cm^{-1}. The O–H stretch in the nanoparticles is due to the secondary metabolites such as polyphenols, sugars, amino acids which have been reported to be responsible for chelation and bio reduction of Fe^{3+} and Fe^{2+} to Fe^0 [7, 14, 29, 40, 43]. These also explains their roles as capping agents as they are also observed in spectra of iron nanoparticles, though there was a slight shift in the vibrational frequencies observed. The peaks at 1027 cm^{-1}, 1037.7 cm^{-1} and 1031 cm^{-1} in CbNPs, GpNPs and BpNPs and at 1000 cm^{-1} for the extracts respectively are due to C–O-C vibrational frequencies of glycosidic linkage in the extracts [44]. Those in 1400 cm^{-1} for the nanoparticles are assigned to the C–C and C=C for aromatic stretching [7]. The bands at 1631, 1630 and 1627.4 cm^{-1} in BpNPS, CbNPs and GpNPs respectively indicate the presence of C=C vibrational mode for unsaturated metabolites such as terpenoids. The iron-oxygen bond observed at 671 cm^{-1}, 621 cm^{-1} and 636 cm^{-1} (Fig. 6) [13, 28, 29, 45-48]. The FTIR bands for the synthesized iron nanoparticles matched well with those for their respective plant extracts, which demonstrate that the components present in the extracts capped the synthesized iron nanoparticles. However, shifts in the bands between the nanoparticles and the extracts, weakening in the transmittance as well as disappearance designate that water soluble biomolecules such as reducing sugars and polyphenols are responsible for bio-reduction of Fe^{3+} [28, 49]. The spectra of the iron nanoparticles after degradation of methylene blue in the presence of H_2O_2 are shown in Fig. 7. It was observed that the OH stretch peaks for the used CbNPs, GpNPs and BpNPs nanoparticles shifted from 3406 cm^{-1}, 3438 cm^{-1} and 3402 cm^{-1} to 3337 cm^{-1}, 3320 cm^{-1} and 338 cm^{-1} respectively. The shifts in peak intensity of the nanoparticles after degradation is due
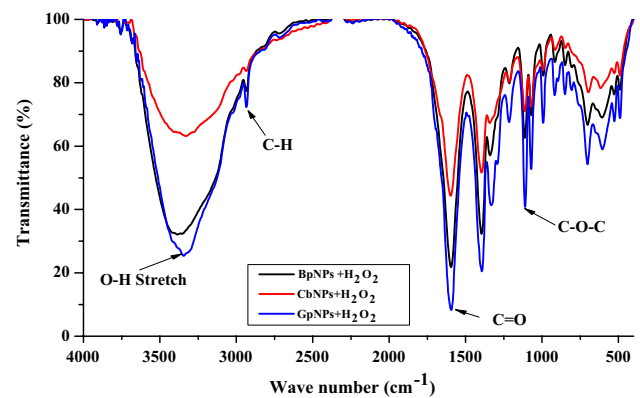
to the photo excitation of the catalyst, which is brought about by the exothermic reaction between the dye, and the hydroxyl groups attached on the surface of the nanoparticles [50, 51].

3.4 X-ray fluorescence analysis

The composition of iron nanoparticles using *Galinsoga parviflora*, *Conyza bonariensis* and *Bidens pilosa* extracts were evaluated using EDXRF and the results are depicted in Fig. 8.

Figure 8 shows the percentage elemental composition obtained from EDXRF quantification of the synthesized plant iron oxide nanoparticles. Plant mediated FeNPs of *Galinsoga parviflora*, *Conyza bonariensis* and *Bidens pilosa* had 51, 47 and 44% of iron respectively. The synthesized Fe particles revealed highest percentage of iron than other elements in the total weight of Fe_3O_4-NPs [13]. The higher percentage of chlorine must have originated from chloride
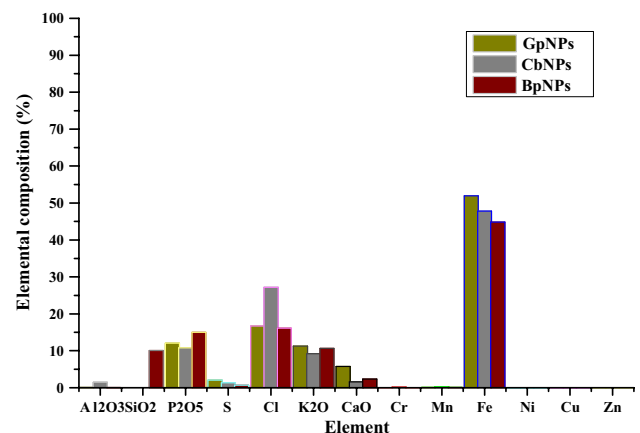

Fig. 8 Elemental composition of the synthesized iron nanoparticles analysed using energy-dispersive X-ray spectrometer of iron oxide nanoparticles

present in aqueous extracts used in the synthesis protocol [30]. Therefore, the elemental analysis of the iron nanoparticles confirmed the synthesis of FeNPs using *Galinsoga parviflora*, *Conyza bonariensis* and *Bidens pilosa* aqueous extracts with impurity peaks of P_2O_5, K_2O and CaO.

3.5 X-ray diffractograms

The X-ray diffractograms obtained for the FeNPs synthesized using *Bidens pilosa*, *Conyza bonariensis* and *Galinsoga parviflora* extract is shown in Figs. 9, 10, 11 respectively.

BpNPs displayed a number of diffraction peaks at 2θ values of 16.03°, 21.44°, 32.73°, 36.45°, 43.75°, 49.46°, 58.39°, and 68.69° while GPNPs had diffraction peaks at 2θ values of 29.89°, 34.20°, 43.13°, 49.02°, 53.17° and 57.95° which are due to a mixture of iron oxides such as magnetite and maghemite [52]. Shoulders depicted at the range of 2θ = 10°–20° at around 20° relates to the presence of polyphenols from leaf extracts as capping and stabilizing agents caused by organic matter [53-55]. Those from 20° to 58° corresponds to the characteristic peaks of a mixture of iron oxides. A typical peak at 36° in BpNPs shows presence magnetite (Fe_3O_4) [14, 40, 48, 52, 56]. CbNPs had an amorphous nature while GpNPs with poor crystallinity due to the amorphous nature hence the diffraction patterns do not depict any distinctive diffraction peaks suggesting that the green synthesis approach resulted in the production of amorphous iron nanoparticles [54, 55, 57].

3.6 SEM micrographs

The SEM micrographs of iron nanoparticles synthesized from *Conyza bonariensis*, *Bidens pilosa,* and *Galinsoga parviflora* aqueous extracts are shown in Fig. 12.

From the SEM micrographs, GpNPs, CbNPs and BpNPs nanoparticles were agglomerated due to presence of various biomolecules, chloride, and potassium compounds
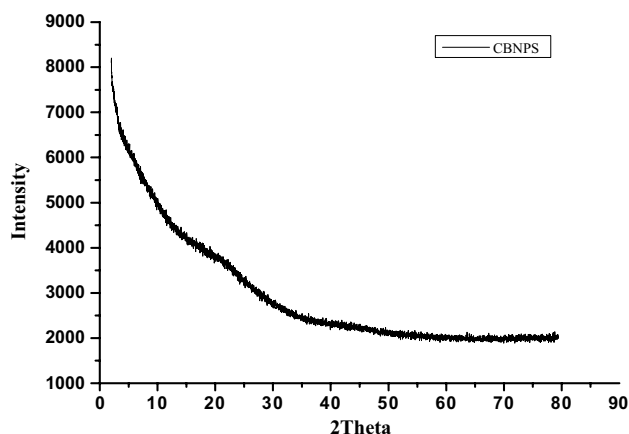
Fig. 10 X-ray diffractogram of CbNPs

present in the leaf extracts which influence the morphology of the nanoparticles [14] and the gold used in sample preparation for SEM analysis [58]. Polyphenols present in the aqueous extracts of *Conyza bonariensis, Bidens pilosa,* and *Galinsoga parviflora* play a vital role as reducing agents and control the agglomeration of the nanoparticles through van der Waals interaction [48, 59].

3.7 Degradation of methylene blue

The nanoparticles were investigated for their ability to catalyze degradation of methylene blue dye and the results are depicted in Figs. 13, 14, 15 [50]. The catalytic activity of the hydrogen peroxide, the nanoparticles without hydrogen peroxide as controls, were also evaluated for 40 min each as shown in Figs. 15, 16.

Hydrogen peroxide, GpNPs, CbNPs and BpNPs degraded the methylene blue by 6.85%, 0.4710%, 0.549% and 2.129% respectively. Their rate constants were found to be 5.60×10^{-4}, 1.35×10^{-4}, 1.70×10^{-5}, and
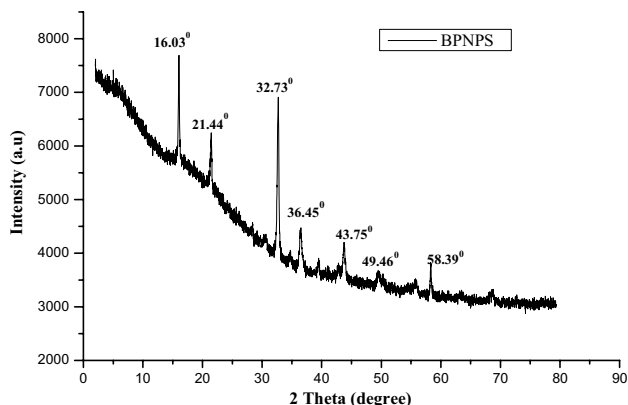
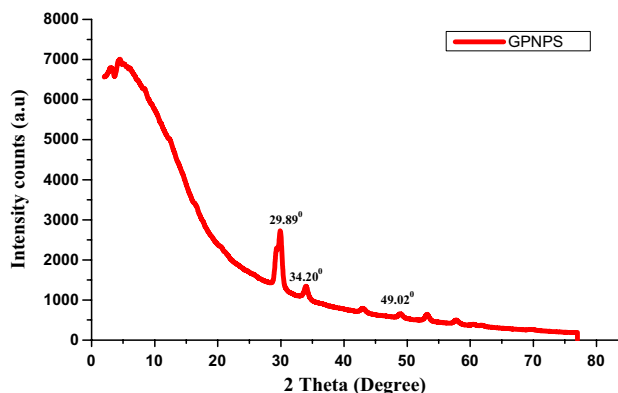**Fig. 9** X-ray diffractogram of BpNPs

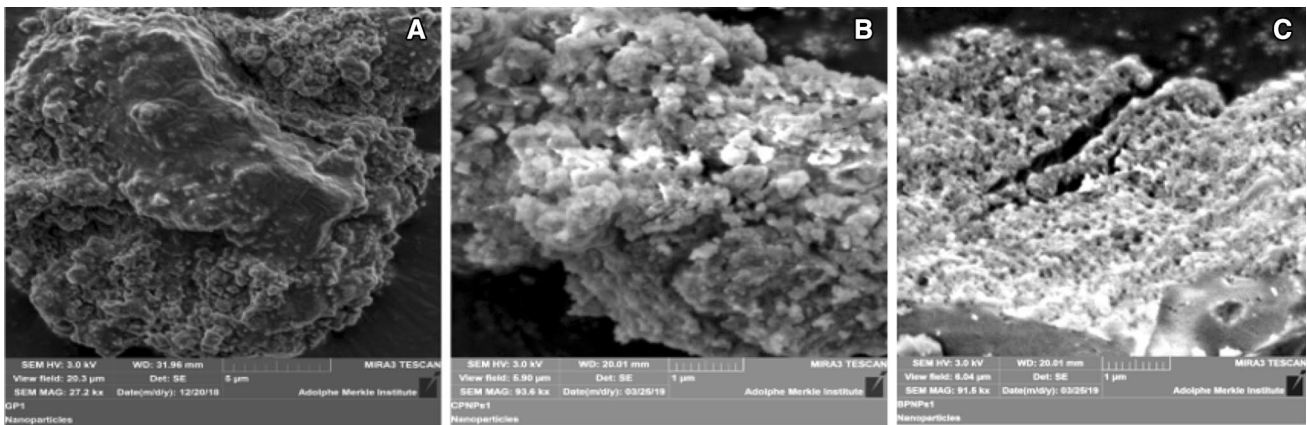**Fig. 11** XRD diffractogram of GpNPs

Fig. 12 SEM images of synthesized GpNPs (**a**), CbNPs (**b**), and BpNPs (**c**) iron nanoparticles (FeNPs)

Fig. 13 Kinetics of methylene blue degradation using CbNPs/H_2O_2. Insert time dependent UV–Vis absorption spectra of methylene blue degradation

Fig. 15 Kinetics of methylene blue degradation using BbNPs/H_2O_2. Insert time dependent UV–Vis absorption spectra of methylene blue degradation
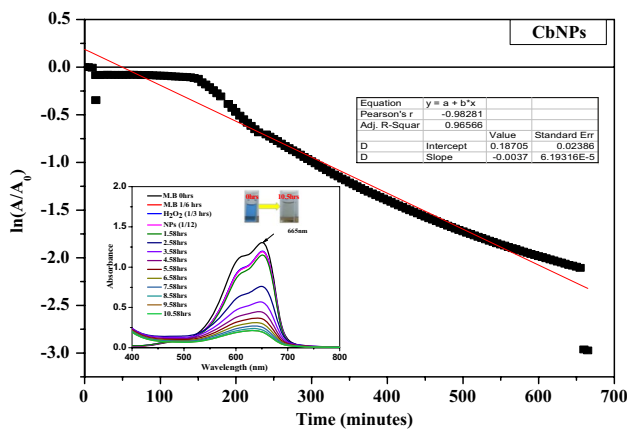

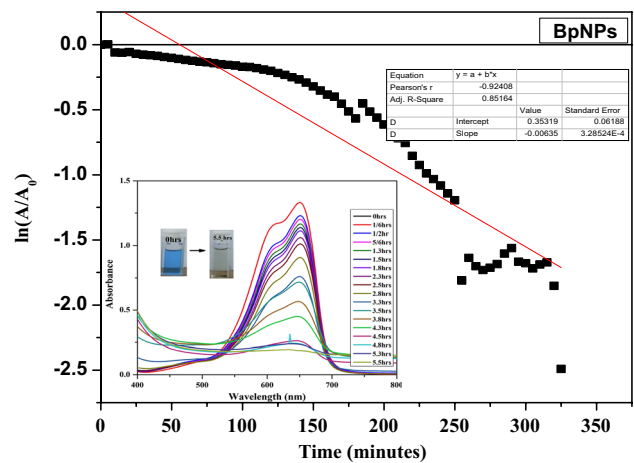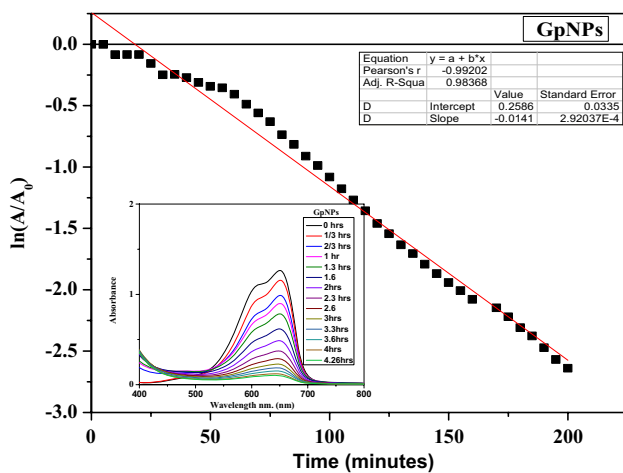**Fig. 14** Kinetics of methylene blue degradation using GpNPs/H_2O_2. Insert time dependent UV–Vis absorption spectra of methylene blue degradation
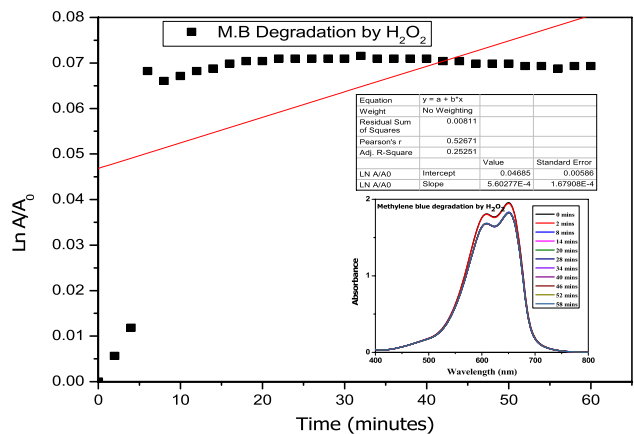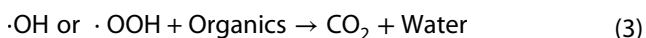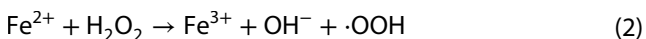

Fig. 16 Kinetics of methylene blue degradation using H_2O_2. Insert time dependent UV–Vis absorption spectra of methylene blue degradation

2.82×10^{-4} respectively. The absorption rate of methylene blue (M.B) remained the same for about 20 min, but upon addition of hydrogen peroxide, there was a small drop in absorption spectra due degradation of the dye by hydrogen peroxide. Addition of the iron nanoparticles provoked further methylene blue degradation for variable contact times. Since absorbance is directly proportional to concentration, the percentage degradation was calculated using the formula: $((A_0 - A)/A_0) * 100\%$. The order of reaction was determined using the plots of $\ln A/A_0$ against time. The degradation rate constant (K) is the slope of the graphs. A_O is the initial absorbance while A is the final absorption. The CbNPs, BpNPs and GpNPs degraded methylene blue by 86.2%, 84.3% and 92.9% for 10.5 h, 5.5 h and 4.3 h and the first order rate constants obtained from a plot of $\ln A/A_0$ against time were 3.77×10^{-3}, 8.35×10^{-3}, and 1.456×10^{-3} per minute respectively [60]. The use of iron nanoparticles alone had no appreciable effect on the absorbance while use of hydrogen peroxide caused a slight change. The catalytic activity of the iron nanoparticles is due to the Fenton and Fenton-like mechanisms. The ferric cations can be reduced to ferrous cations through reaction with the electrons produced from photoreactions. The ferrous ions are reoxidized back to ferric by the hydrogen peroxide resulting in production of ($\cdot$OH) radicals through photo Fenton reaction. Hydroxyl radicals ($\cdot$OH) are generated due to the presence of iron ions and hydrogen peroxide. The $\cdot$OH radicals together with the H^+ and $\cdot O_2^-$ play the role of degradation of the methylene blue dye when coupled as $H^+ + \cdot O_2^-$ and $H^+ + (\cdot OH)$ [61].

$$Fe^{3+} + H_2O_2/e^- \rightarrow Fe^{2+} + OH^- + \cdot OH \qquad (1)$$

$$Fe^{2+} + H_2O_2 \rightarrow Fe^{3+} + OH^- + \cdot OOH \qquad (2)$$

$$\cdot OH \text{ or } \cdot OOH + Organics \rightarrow CO_2 + Water \qquad (3)$$

Generation of the radicals involves the electronic transitions between iron and oxygen in the particles which leads to an exciton emission (electron) in the valence band, consisting of Fe ($3d$) and O ($2p$) being excited to the conduction band that consists of Fe ($4s$ and $3d$) and O ($2p$). These create a positively charged hole in the valence band and negatively charged conduction band, which reacts with hydrogen peroxide and water producing reactive hydroxyl radicals The radicals break down the organic compounds into carbon dioxide and water. The intermediates iron produced such as Fe $^{2+}$, Fe $^{3+}$, their hydroxides are thermodynamically unstable and much active. These also contributes to the catalytic activity [61–65]. Therefore, the radicals react with methylene blue resulting in dye degradation [34, 50, 60].

4 Conclusion

Aqueous extracts of *Galinsoga Parviflora*, *Bidens pilosa* and *Conyza bonariensis* leaves can be used for the biosynthesis of iron oxide nanoparticles. Functional group analysis, and elemental composition of the particles revealed that the nanoparticles were largely composed of iron with oxygen bearing functional groups. Application of the synthesized nanoparticles as a catalyst against methylene blue degradation revealed that while the particles were able to degrade the dye, the rate of degradation was dependent on the extracts used during synthesis. Different nanoparticles had different degradation rates, but they all followed first order rate reaction. Hence, the aqueous extracts from the three plants can be used to synthesize iron nanoparticles which can be used as catalysts in the degradation of dyes with hydrogen peroxide at different reaction rates.

Compliance with ethical standards

References

1. Seigneuric R, Markey L, Nuyten DS, Dubernet C, Evelo CT, Finot E, Garrido C (2010) From nanotechnology to nanomedicine: applications to cancer research. Curr Mol Med 10:640–652. https://doi.org/10.2174/156652410792630634

2. Shameli K, Bin Ahmad M, Yunus WMZW, Rustaiyan A, Ibrahim NA, Zargar M, Abdollahi Y (2010) Green synthesis of silver/montmorillonite/chitosan bionanocomposites using the UV irradiation method and evaluation of antibacterial activity. Int J Nanomed 5:875–887. https://doi.org/10.2147/IJN.S13632

3. Govindarajan M, Benelli G (2017) A facile one-pot synthesis of eco-friendly nanoparticles using *Carissa carandas*: ovicidal and larvicidal potential on malaria dengue and filariasis mosquito vectors. J Clust Sci 28:15–36. https://doi.org/10.1007/s10876-016-1035-6

4. Benelli G (2016) Plant-mediated biosynthesis of nanoparticles as an emerging tool against mosquitoes of medical and veterinary importance: a review. Parasitol Res 115:23–34. https://doi.org/10.1007/s00436-015-4800-9

5. Dinesh D, Murugan K, Madhiyazhagan P, Panneerselvam C, Mahesh Kumar P, Nicoletti M, Jiang W, Benelli G, Chandramohan B, Suresh U (2015) Mosquitocidal and antibacterial activity of green-synthesized silver nanoparticles from aloe vera extracts: towards an effective tool against the malaria vector *Anopheles stephensi*? Parasitol Res 114:1519–1529. https://doi.org/10.1007/s00436-015-4336-z

6. Shaik M, Ali Z, Khan M, Kuniyil M, Assal M, Alkhathlan H, Al-Warthan A, Siddiqui M, Khan M, Adil S (2017) Green synthesis and characterization of palladium nanoparticles using *Origanum*

vulgare L. extract and their catalytic activity, Molecules 22:165. https://doi.org/10.3390/molecules22010165

7. Izadiyan Z, Shameli K, Miyake M, Hara H, Mohamad SEB, Kalantari K, Taib SHM, Rasouli E (2018) Cytotoxicity assay of plant-mediated synthesized iron oxide nanoparticles using *Juglans regia* green husk extract. Arab J Chem. https://doi.org/10.1016/j.arabjc.2018.02.019

8. Devatha CP, Thalla AK, Katte SY (2016) Green synthesis of iron nanoparticles using different leaf extracts for treatment of domestic waste water. J Clean Prod. https://doi.org/10.1016/j.jclepro.2016.09.019

9. Yew YP, Shameli K, Miyake M, Kuwano N, Bt Ahmad Khairudin NB, Bt Mohamad SE, Lee K.X (2016) Green synthesis of magnetite (Fe3O4) nanoparticles using seaweed (*Kappaphycus alvarezii*) extract. Nanoscale Res Lett. https://doi.org/10.1186/s11671-016-1498-2.

10. Karaman DŞ, Manner S, Fallarero A, Rosenholm JM (2017) Current approaches for exploration of nanoparticles as antibacterial agents. Antibact Agents. https://doi.org/10.5772/68138

11. Slavin YN, Asnis J, Häfeli UO, Bach H (2017) Metal nanoparticles: understanding the mechanisms behind antibacterial activity. J Nanobiotechnol 15:1–20. https://doi.org/10.1186/s12951-017-0308-z

12. Fernando SSN, Gunasekara T, Holton J (2018) Antimicrobial nanoparticles: applications and mechanisms of action. Sri Lankan J Infect Dis 8(2):11

13. Kanagasubbulakshmi S, Kadirvelu K (2017) Green synthesis of iron oxide nanoparticles using *Lagenaria siceraria* and evaluation of its antimicrobial activity. Def Life Sci J 2:422–427

14. Groiss S, Selvaraj R, Varadavenkatesan T, Vinayagam R (2017) Structural characterization, antibacterial and catalytic effect of iron oxide nanoparticles synthesised using the leaf extract of *Cynometra ramiflora*. J Mol Struct. https://doi.org/10.1016/j.molstruc.2016.09.031

15. Yuan C-G, Huo C, Gui B, Cao W-P (2017) Green synthesis of gold nanoparticles using citrus maxima peel extract and their catalytic/antibacterial activities. IET Nanobiotechnol 11:523–530. https://doi.org/10.1049/iet-nbt.2016.0183

16. Saif S, Tahir A, Chen Y (2016) Green synthesis of iron nanoparticles and their environmental applications and implications. Nanomaterials. https://doi.org/10.3390/nano6110209

17. Silveira C, Shimabuku QL, Fernandes Silva M, Bergamasco R (2017) Iron-oxide nanoparticles by green synthesis method using Moringa oleifera leaf extract for fluoride removal. Environ Technol. 3330:1–40. https://doi.org/10.1080/09593330.2017.1369582.

18. Sravanthi K, Ayodhya D, Yadgiri Swamy P (2018) Green synthesis, characterization of biomaterial-supported zero-valent iron nanoparticles for contaminated water treatment. J Anal Sci Technol. 9:3. https://doi.org/10.1186/s40543-017-0134-9.

19. Wang C (2007) Photocatalytic activity of nanoparticle gold/iron oxide aerogels for azo dye degradation. J Non-Cryst Solids 353(1126):1133. https://doi.org/10.1016/j.jnoncrysol.2006.12.028

20. Makarov VV, Makarova SS, Love AJ, Sinitsyna OV, Dudnik AO, Yaminsky IV, Taliansky ME, Kalinina NO (2014) Biosynthesis of stable iron oxide nanoparticles in aqueous extracts of *Hordeum vulgare* and *Rumex acetosa* plants. Langmuir 30:5982–5988. https://doi.org/10.1021/la5011924

21. Devatha CP, Jagadeesh K, Patil M (2018) Effect of green synthesized iron nanoparticles by Azardirachta Indica in different proportions on antibacterial activity. Environ Nanotechnol Monit Manag. https://doi.org/10.1016/j.enmm.2017.11.007

22. Murgueitio E, Cumbal L, Abril M, Izquierdo A, Debut A, Tinoco O (2018) Green synthesis of iron nanoparticles: application on the removal of petroleum oil from contaminated water and soils. J Nanotechnol. https://doi.org/10.1155/2018/4184769.

23. Igwe OU, Nwamezie F (2018) Green synthesis of iron nanoparticles using flower extract of Piliostigma thonningii and their antibacterial activity evaluation. Chem Int 4:60–66

24. Ruto MC, Ngugi CM, Kareru PG, Cheruiyot K, Rechab SO, Madivoli ES, Mutembei JK, Kairigo PK, Maina EG (2018) Antioxidant activity and antimicrobial properties of *Entada leptostachya* and *Prosopis juliflora* extracts. J Med Plants Econ Dev 2:8. https://doi.org/10.4102/jomped.v2i1.31

25. Baba SA, Malik SA (2015) Determination of total phenolic and flavonoid content, antimicrobial and antioxidant activity of a root extract of *Arisaema jacquemontii* blume. J Taibah Univ Sci 9:449–454. https://doi.org/10.1016/j.jtusci.2014.11.001

26. Parimelazhagan T (2016) Pharmacological Assays of Plant-Based Natural Products. https://doi.org/10.1007/978-3-319-26811-8

27. Baba SA, Malik SA (2014) Evaluation of antioxidant and antibacterial activity of methanolic extracts of Gentiana kurroo royle. Saudi J Biol Sci 21:493–498. https://doi.org/10.1016/j.sjbs.2014.06.004

28. Jeyasundari J, Praba PS, Jacob YBA, Vasantha VS, Shanmugaiah V (2017) Green synthesis and characterization of zero valent iron nanoparticles from the leaf Extract of *Psidium guajava* plant and their antibacterial activity. Chem Sci Rev Lett 6:1244–1252

29. Fazlzadeh M, Rahmani K, Zarei A, Abdoallahzadeh H, Nasiri F, Khosravi R (2017) A novel green synthesis of zero valent iron nanoparticles (NZVI) using three plant extracts and their efficient application for removal of Cr(VI) from aqueous solutions. Adv Powder Technol 28:122–130. https://doi.org/10.1016/j.apt.2016.09.003

30. Balamurugan M, Saravanan S, Soga T (2014) Synthesis of iron oxide nanoparticles by using *Eucalyptus Globulus* plant extract. E-Journal Surf Sci Nanotechnol 12:363–367. https://doi.org/10.1380/ejssnt.2014.363

31. Borja JQ, Ngo MAS, Saranglao CC, Tiongco RPM, Roque EC, Dugos NP (2015) Synthesis of green zero-valent iron using polyphenols from dried green tea extract. J Eng Sci Technol 10:22–31

32. Siddiqi KS, ur Rahman A, Tajuddin, Husen A (2016) Biogenic fabrication of iron/iron oxide nanoparticles and their application. Nanosc Res Lett https://doi.org/10.1186/s11671-016-1714-0

33. Ponce C, Chanona J, Garibay V, Palacios E, Calderon G, Sabo R (2013) Functionalization of agave cellulose nanoparticles and its characterization by microscopy and spectroscopy techniques. Microsc Microanal 19:200–201. https://doi.org/10.1017/S1431927613002997

34. Lassoued A, Saber M, Brahim L, Salah D, Abdellatif A (2018) Photocatalytic degradation of methylene blue dye by iron oxide (α-Fe_2O_3) nanoparticles under visible irradiation. J Mater Sci Mater Electron. https://doi.org/10.1007/s10854-018-8819-4

35. Velusamy P, Kumar GV, Jeyanthi V, Das J, Pachaiappan R (2016) Bio-inspired green nanoparticles: synthesis, mechanism, and antibacterial application. Toxicol Res 32:95–102. https://doi.org/10.5487/TR.2016.32.2.095

36. Kaushik U, Joshi SC (2015) Silver nanoparticles: Green synthesis, optical properties, antimicrobial activity and its mechanism using *Citrus sinensis*. Asian J Pharm Clin Res 8:179–184

37. Journal AI, Yadi M, Mostafavi E, Saleh B, Davaran S, Khalilov R, Nikzamir M, Nikzamir N, Panahi Y, Milani M (2018) Current developments in green synthesis of metallic nanoparticles using plant extracts: a review. Artif Cells Nanomed Biotechnol 0:1–8. https://doi.org/10.1080/21691401.2018.1492931

38. Makarov VV, Love AJ, Sinitsyna OV, Makarova SS, Yaminsky IV, Taliansky ME, Kalinina NO (2014) "Green" nanotechnologies: synthesis of metal nanoparticles using plants. Acta Naturae 6:35–44. https://doi.org/10.1039/c1gc15386b

39. Iravani S (2016) Green synthesis of metal nanoparticles using plants. Green Chem. https://doi.org/10.1039/C1GC15386B

40. Huang L, Weng X, Chen Z, Megharaj M, Naidu R (2014) Synthesis of iron-based nanoparticles using oolong tea extract for the degradation of malachite green. Spectrochim Acta Part A Mol Biomol Spectrosc. https://doi.org/10.1016/j.saa.2013.09.054.

41. Alam MN, Bristi NJ, Rafiquzzaman M (2013) Review on in vivo and in vitro methods evaluation of antioxidant activity. Saudi Pharm J 21:143–152. https://doi.org/10.1016/j.jsps.2012.05.002

42. Da'na E, Taha A, Afkar E (2018) Green synthesis of iron nanoparticles by acacia nilotica pods extract and its catalytic, adsorption, and antibacterial activities. Appl Sci. 8:1922. https://doi.org/10.3390/app8101922.

43. Azam A, Habib SS, Memic A, Ahmed AS, Oves M, Khan MS (2012) Antimicrobial activity of metal oxide nanoparticles against gram-positive and gram-negative bacteria: a comparative study. Int J Nanomed 7:6003–6009. https://doi.org/10.2147/IJN.S35347

44. Mashjoor S, Yousefzadi M, Zolgharnain H, Kamrani E, Alishahi M (2018) Organic and inorganic nano-Fe_3O_4: Alga Ulva flexuosa-based synthesis, antimicrobial effects and acute toxicity to briny water rotifer Brachionus rotundiformis. Environ Pollut 237:50–64. https://doi.org/10.1016/j.envpol.2018.02.036

45. Jagathesan G, Rajiv P (2018) Biosynthesis and characterization of iron oxide nanoparticles using Eichhornia crassipes leaf extract and assessing their antibacterial activity. Biocatal Agric Biotechnol 13:90–94. https://doi.org/10.1016/j.bcab.2017.11.014

46. Hwang SW, Umar A, Dar GN, Kim SH, Badran RI (2014) Synthesis and characterization of iron oxide nanoparticles for phenyl hydrazine sensor applications. Sens Lett 12:97–101. https://doi.org/10.1166/sl.2014.3224

47. Betancur AF, Pérez FR, Correa MM, Barrero CA (2012) Quantitative approach in iron oxides and oxihydroxides by vibrational analysis Aproximación cuantitativa en óxidos y oxihidróxidos de hierro mediante análisis vibracional. Opt Pura y Apl 878:269–275. https://doi.org/10.7149/OPA.45.3.269

48. Wang T, Jin X, Chen Z, Megharaj M, Naidu R (2014) Green synthesis of Fe nanoparticles using eucalyptus leaf extracts for treatment of eutrophic wastewater. Sci Total Environ 466–467:210–213. https://doi.org/10.1016/j.scitotenv.2013.07.022

49. Xiao Z, Yuan M, Yang B, Liu Z, Huang J, Sun D (2016) Plant-mediated synthesis of highly active iron nanoparticles for Cr(VI) removal: investigation of the leading biomolecules. Chemosphere 150:357–364. https://doi.org/10.1016/j.chemosphere.2016.02.056

50. Chauhan R, Kumar A, Pal R (2013) Photocatalytic degradation of methylene blue with Fe doped ZnS nanoparticles. Spectrochim Acta Part A Mol Biomol Spectrosc 113:250–256. https://doi.org/10.1016/j.saa.2013.04.087

51. Kushwaha R (2018) Degradation of Nile blue sulphate dye onto iron oxide nanoparticles: kinetic study, identification of reaction intermediates, and proposed mechanistic pathways. Asia-Pac J Chem Eng. https://doi.org/10.1002/apj.2200.

52. Mishra D, Arora R, Lahiri S, Amritphale SS, Chandra N (2014) Synthesis and characterization of iron oxide nanoparticles by solvothermal method. Prot Met Phys Chem Surf 50:628–631. https://doi.org/10.1134/s2070205114050128

53. Soliemanzadeh A, Fekri M, Bakhtiary S, Mehrizi MH (2016) Biosynthesis of iron nanoparticles and their application in removing phosphorus from aqueous solutions. Chem Ecol 32:286–300. https://doi.org/10.1080/02757540.2016.1139091

54. Wang Z, Fang C, Megharaj M (2014) Characterization of iron-polyphenol nanoparticles synthesized by three plant extracts and their fenton oxidation of azo dye. ACS Sustain Chem Eng 2:1022–1025. https://doi.org/10.1021/sc500021n

55. Ebrahiminezhad A, Zare-Hoseinabadi A, Berenjian A, Ghasemi Y (2017) Green synthesis and characterization of zero-valent iron nanoparticles using stinging nettle (Urtica dioica) leaf extract. Green Process Synth 6:469–475. https://doi.org/10.1515/gps-2016-0133

56. Al-Kalifawi EJ (2015) Green synthesis of magnetite iron oxide nanoparticles by using Al-Abbas's (A.S.) hund fruit (Citrus medica) var. sarcodactylis swingle extract and used in Al-'alqami river water treatment. J Nat Sci Res 5:125–135

57. Veeramanikandan V, Madhu GC, Pavithra V, Jaianand K, Balaji P (2017) Green Synthesis, characterization of iron oxide nanoparticles using Leucas aspera leaf extract and evaluation of antibacterial and antioxidant studies. Int J Agric Innov Res 6:242–250

58. Predescu AM, Matei E, Berbecaru AC, Pantilimon C, Drăgan C, Vidu R, Predescu C, Kuncser V (2018) Synthesis and characterization of dextran-coated iron oxide nanoparticles. R Soc Open Sci. https://doi.org/10.1098/rsos.171525

59. Sulaiman GM, Tawfeeq AT, Naji AS (2018) Biosynthesis, characterization of magnetic iron oxide nanoparticles and evaluations of the cytotoxicity and DNA damage of human breast carcinoma cell lines. Artif Cells Nanomed Biotechnol 46:1215–1229. https://doi.org/10.1080/21691401.2017.1366335

60. Shah A, Haq S, Rehman W, Waseem M, Shoukat S (2019) Photocatalytic and antibacterial activities of paeonia emodi mediated silver oxide nanoparticles. Mater Res Express 6:45045. https://doi.org/10.1088/2053-1591/aafd42

61. Chang F, Wu F, Zheng JJ, Cheng W, Yan W, Deng B, Hu X (2018) In-situ establishment of binary composites A-Fe_2O_3/$Bi_{12}O_{17}Cl_2$ with both photocatalytic and photo-Fenton features. Chemosphere 210:257–266. https://doi.org/10.1016/j.chemosphere.2018.07.010

62. Önal ES, Yatkin T, Ergüt M, Özer A (2017) Green synthesis of iron nanoparticles by aqueous extract of Eriobotrya japonica leaves as a heterogeneous fenton-like catalyst: degradation of basic red 46. Int J Chem Eng Appl 8:327–333. https://doi.org/10.18178/ijcea.2017.8.5.678

63. El-Sayed EM, Elkady MF, El-Latif MMA (2017) Biosynthesis and characterization of zerovalent iron nanoparticles and its application in azo dye degradation. Indian J Chem Technol 24:541–547

64. He D, Wu X, Chen Y, Situ Y, Zhong L, Huang H (2018) In-situ growth of lepidocrocite on Bi_2O_3 rod: aperfect cycle coupling photocatalysis and heterogeneous fenton-like process by potential-level matching with advanced oxidation. Chemosphere 210:334–340. https://doi.org/10.1016/j.chemosphere.2018.06.142

65. Wan D, Zuo J, Chen Y, Chen Q, Zuo Y (2018) Photodegradation of amitriptyline in Fe(III)-citrate-oxalate binary system: synergistic effect and mechanism. Chemosphere 210:224–231. https://doi.org/10.1016/j.chemosphere.2018.07.006